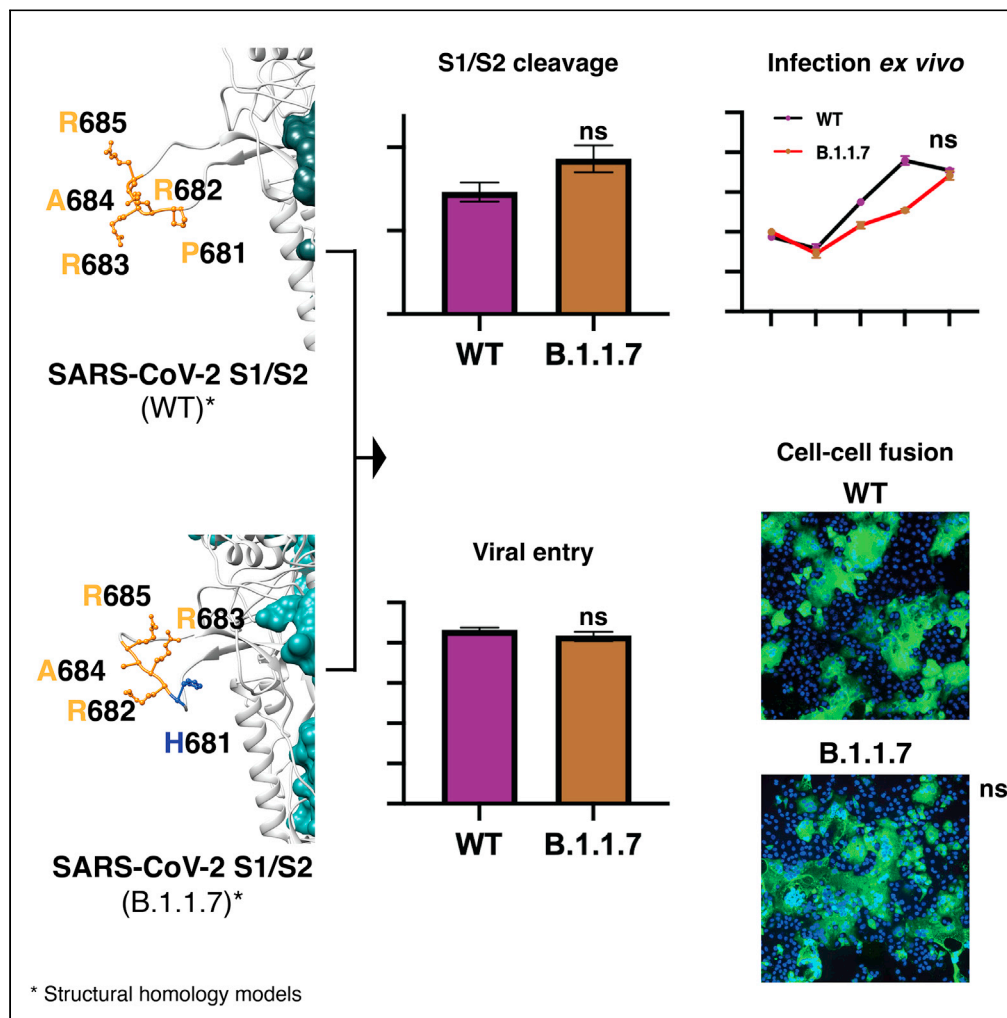


Article

Functional evaluation of the P681H mutation on the proteolytic activation of the SARS-CoV-2 variant B.1.1.7 (Alpha) spike



Bailey Lubinski, Maureen H.V. Fernandes, Laura Frazier, ..., Diego G. Diel, Javier A. Jaimes, Gary R. Whittaker

jaj246@cornell.edu (J.A.J.)
grw7@cornell.edu (G.R.W.)

Highlights

SARS-CoV-2 B.1.1.7 P681H mutation in the spike is predicted to enhance viral infection

P681H does not significantly impact furin cleavage, viral entry, or cell-cell spread

Other mutations in the SARS-CoV-2 B.1.1.7 VOC may account for increased infection rates



Article

Functional evaluation of the P681H mutation on the proteolytic activation of the SARS-CoV-2 variant B.1.1.7 (Alpha) spike

Bailey Lubinski,¹ Maureen H.V. Fernandes,² Laura Frazier,¹ Tiffany Tang,³ Susan Daniel,³ Diego G. Diel,² Javier A. Jaimes,^{1,*} and Gary R. Whittaker^{1,4,5,*}

SUMMARY

Severe acute respiratory syndrome coronavirus 2 (SARS-CoV-2) is the agent causing the COVID-19 pandemic. SARS-CoV-2 B.1.1.7 (Alpha), a WHO variant of concern first identified in the United Kingdom in late 2020, contains several mutations including P681H in the spike S1/S2 cleavage site, which is predicted to increase cleavage by furin, potentially impacting the viral cell entry. Here, we studied the role of the P681H mutation in B.1.1.7 cell entry. We performed assays using fluorogenic peptides mimicking the Wuhan-Hu-1 and B.1.1.7 S1/S2 sequence and observed no significant difference in furin cleavage. Functional assays using pseudoparticles harboring SARS-CoV-2 spikes and cell-to-cell fusion assays demonstrated no differences between Wuhan-Hu-1, B.1.1.7, or a P681H point mutant. Likewise, we observed no differences in viral growth between USA-WA1/2020 and a B.1.1.7 isolate in cell culture. Our findings suggest that, although the B.1.1.7 P681H mutation may slightly increase S1/S2 cleavage, this does not significantly impact viral entry or cell-cell spread.

INTRODUCTION

Severe acute respiratory syndrome coronavirus 2 (SARS-CoV-2) is the agent behind the current COVID-19 pandemic (Whittaker et al., 2021). SARS-CoV-2 emerged from a yet to be determined animal reservoir and was first identified in late 2019; it has since rapidly spread throughout the world. The virus now exists in two lineages, A and B. Although both lineages remain in circulation globally, the B lineage became the dominant virus following its introduction into Northern Italy in February 2020. The B lineage has undergone significant diversification as it expanded and in particular acquired an S gene mutation (D614G) that resulted in a more stabilized spike protein, which has been linked to increased transmissibility (Zhou et al., 2021). D614G has now become established in circulating B lineage viruses.

In late summer to early fall 2020, a new variant of SARS-CoV-2 was identified in the United Kingdom, based on S-gene target failures in community-based diagnostic PCR testing (Rambaut et al., 2020). Following subsequent sequence analysis, this variant was defined as variant of concern (VOC) B.1.1.7/501Y.V1 by Public Health England and later denominated as the Alpha variant. B.1.1.7 rapidly expanded across the south of England and subsequently spread to other parts of the United Kingdom (Volz et al., 2021), and then globally. The B.1.1.7 VOC was unusual compared with other SARS-CoV-2 variants emerging at that time in that it contained a higher than typical level of point mutants across its genome, 23 in total. Of particular note were nine mutations in the spike gene compared with prototype sequences: a 69-70 deletion, Y144 del, N501Y, A570D, D614G, P681H, T716I, S982A, and D118H, with seven of these distinct to B.1.1.7. One of the more concerning mutations was N501Y, which was linked (along with D614G) to increased affinity of the spike protein to the SARS-CoV-2 receptor, angiotensin converting enzyme 2 (ACE2). N501Y has subsequently been found in other VOCs circulating around the world, i.e., B.1.351 and B.1.1.28.1 (P.1) (Coutinho et al., 2021; Lauring and Hodcroft, 2021; Tegally et al., 2021a).

Since its first identification, SARS-CoV-2 B.1.1.7 has undergone extensive characterization. Current consensus indicates that this VOC has a transmission advantage in the community (Davies et al., 2021; Volz et al., 2021), possibly accompanied by increased disease severity (Challen et al., 2021), but it does not appear to evade immune surveillance by natural immunity or vaccination. One hypothesis is that the B.1.1.7 variant acquired its

¹Department of Microbiology & Immunology, College of Veterinary Medicine, Cornell University, 618 Tower Road, Ithaca, NY 14853, USA

²Department of Population Medicine, College of Veterinary Medicine, Cornell University, Ithaca, NY 14853, USA

³Robert Frederick Smith School of Chemical & Biomolecular Engineering, Cornell University, Ithaca, NY 14853, USA

⁴Master of Public Health Program, Cornell University, Ithaca, NY 14853, USA

⁵Lead contact

*Correspondence: jaj246@cornell.edu (J.A.J.), grw7@cornell.edu (G.R.W.)
<https://doi.org/10.1016/j.isci.2021.103589>



extensive range of mutations in a single immunocompromised individual (Rambaut et al., 2020) who then initiated a super-spreader event that gave rise to the subsequent dissemination of the lineage.

The P681H mutation of B.1.1.7 is of note as it is part of a proteolytic cleavage site for furin and furin-like proteases at the junction of the spike protein receptor-binding (S1) and fusion (S2) domains (Jaimes et al., 2020a). The S1/S2 junction of the SARS-CoV-2 S gene has a distinct indel compared with all other SARS-like viruses (*Sarbecoviruses* in *Betacoronavirus* lineage B); the amino acid sequence of SARS-CoV-2 S protein is $_{681}\text{-P-R-R-A-R}\text{S}_{-686}$ with proteolytic cleavage (|) predicted to occur between the arginine and serine residues depicted. Based on nomenclature established for proteolytic events (Polgár, 1989), the R|S residues are defined as the P1|P1' residues for enzymatic cleavage, with 681H of B.1.1.7 S being the P5 cleavage position. The ubiquitously expressed serine protease furin is highly specific and cleaves at a distinct multi-basic motif containing paired arginine (R) residues; furin requires a minimal motif of R-X-X-R (P4-X-X-P1), with a preference for an additional basic residue (histidine, H or lysine, K) at P2; i.e., R-X-K/H-R (Seidah and Prat, 2012). For SARS-CoV-2, the presence of the S1/S2 "furin site" enhances virus transmissibility (Johnson et al., 2021; Peacock et al., 2020). For B.1.1.7 S, P681H (P5) may provide an additional basic residue (especially at low pH) and modulate S1/S2 cleavability by furin, and hence virus infection properties.

We previously studied the role of proteolytic activation of the spike protein of the prototype lineage B SARS-CoV-2 (isolate Wuhan-Hu-1) (Tang et al., 2021). Here, we used a similar approach to study the role of the proteolytic activation of the spike protein in the context of the B.1.1.7 VOC, with a focus on the P681H point mutant.

RESULTS

Bioinformatic and biochemical analysis of the SARS-CoV-2 B.1.1.7 S1/S2 cleavage site

To gain insight into proteolytic processing at the S1/S2 site of the B.1.1.7 spike protein, we first took a bioinformatic approach utilizing the PiTou (Tian et al., 2012) and ProP (Duckert et al., 2004) cleavage prediction tools, comparing B.1.1.7 with the prototype virus Wuhan-Hu-1 as well as to SARS-CoV, MERS-CoV, and selected other human respiratory betacoronaviruses (HCoV-HKU1 and HCoV-OC43) (Figure 1A). Both algorithms predicted a limited increase in the furin cleavage for B.1.1.7 compared with Wuhan-Hu-1; in comparison SARS-CoV is not predicted to be furin-cleaved; as expected, MERS-CoV showed a relatively low furin cleavage score with HCoV-HKU1 and HCoV-OC43 showing much higher furin cleavage scores. Previously, we showed that the SARS-CoV-2 S1/S2 cleavage site is predicted to fold as a flexible loop exposed from the spike structure (Jaimes et al., 2020a). Considering that the P681H mutation was predicted to slightly increase the furin cleavage at this site, we modeled the SARS-CoV-2 B.1.1.7 variant spike and observed no marked changes in the predicted folding compared with Wuhan-Hu-1 (Figure 1B).

To directly address the activity of furin on the SARS-CoV-2 B.1.1.7 S1/S2 site, we used a biochemical peptide cleavage assay (Jaimes et al., 2019). The specific peptide sequences used here were TNSHRRARSVA (B.1.1.7 S1/S2) and TNSPRRARSVA (Wuhan-Hu-1 S1/S2). We tested furin, along with trypsin, as a control as described previously (Jaimes et al., 2020b). We also assessed the effect of lowered pH because of the known properties of histidine (H) to have an ionizable side chain with a pKa near neutrality (Nelson and Cox, 2000) (Figure 2A). As predicted, furin effectively cleaved Wuhan-Hu-1 (WT) S1/S2, with B.1.1.7 S1/S2 showing a slight increase in cleavage at pH 7.5. At pH 7.0 and pH 6.5, B.1.1.7 S1/S2 was actually less efficiently cleaved than WT, with cleavage not measurable below pH 6.5 (data not shown). Trypsin cleaved both peptides but was less efficient than furin (at pH 7.4). This comparative data with SARS-CoV S1/S2 sites reveal that the acquisition of the 681H mutation does not significantly increase cleavability by furin and may in fact be inhibitory at lowered pH.

To better understand the role of the P681H mutation in the maturation and activation of the spike protein, we evaluated the expression and cleavage of the SARS-CoV-2 Wuhan-Hu-1 spike protein (WT), along with the B.1.1.7 and a P681H point mutant of Wuhan-Hu-1 spikes via western blot and densitometry. To do this, we used pseudoparticles consisting of a murine leukemia virus (MLV) core displaying the heterologous viral envelope protein. The pseudoparticles were produced under the normal furin conditions or under the presence of the protease inhibitor decanoyl-RVKR-CMK (dec-RVKR-CMK) to produce cleaved and uncleaved S proteins (respectively). The purified pseudoparticles were later incubated with or without furin to better assess furin cleavage. As observed in Figure 2B, partial to full cleavage was observed in all the spikes under normal cellular furin conditions (no dec-RVKR-CMK nor exogenous furin), as well as in furin-incubated particles. Interestingly, the

A	Virus	S1/S2 Sequence	Furin Score PiTou	Furin Score ProP
	SARS-CoV-2 (WT)	672-ASYQTQTNSP RRAR SVASQS-691	+9.196	0.620
	SARS-CoV-2 (B.1.1.7)	669-ASYQTQTNS HRRAR SVASQS-688	+9.907	0.704
	SARS-CoV	654-AGICASYHTVSL LR STSQ KS -673	-5.167	0.123
	MERS-CoV	738-LPDTPSTLTP RSVR SVPGEM-757	+5.155	0.563
	HCoV-HKU1	747-YNSPSSSS RRKR SISASY-766	+14.634	0.918
	HCoV-OC43 (clinical)	750-GYCVDYFK RRSR AITTYG-769	+10.10	0.736

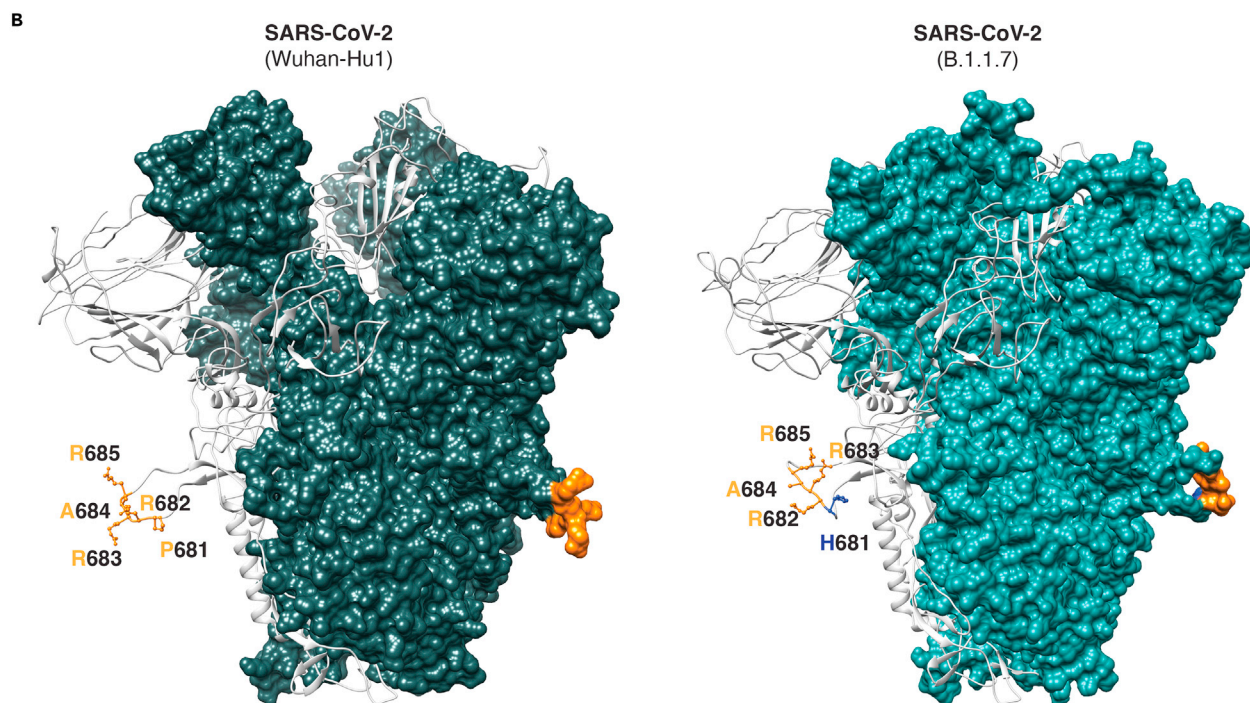


Figure 1. SARS-CoV-2 spike S1/S2 cleavage site

(A) Furin cleavage score analysis of CoV S1/S2 cleavage sites. CoV S sequences were analyzed using the ProP 1.0 and PiTou 3.0 furin prediction algorithm, generating a score with bold numbers indicating predicted furin cleavage. (|) denotes the position of the predicted S1/S2 cleavage site. Basic residues, arginine (R) and lysine (K), are highlighted in blue, with histidine in purple. Sequences corresponding to the S1/S2 region of SARS-CoV-2 (GenBank: QHD43416.1), SARS-CoV (GenBank: AAT74874.1), MERS-CoV (GenBank: AFS88936.1), HCoV-HKU1 (GenBank: AAT98580.1), HCoV-OC43 (GenBank: KY369907.1) and SARS-CoV-2 B.1.1.7 (GISAID: EPI_ISL_1374509) were obtained from open access data bases.

(B) SARS-CoV-2 spike structural models. Homology models were built for the spike protein from Wuhan-Hu1 (WT) and B.1.1.7 variants. The S1/S2 cleavage site sequences are noted. WT sequence ${}_{681}PRRAR_{685}$ is noted in orange and mutated residue H681 is noted in blue. Sequence information is available in Table 1.

addition of the dec-RVCR-CMK inhibitor resulted in almost 100% uncleaved spike in WT but partially cleaved spikes in B.1.1.7 and the P681R mutant. This was also observed when these particles were incubated with exogenous furin, suggesting that the P681H mutation may increase furin cleavage in the complete spike. We then calculated the cleaved S versus uncleaved S ratio for all these spikes. These data were normalized to the expression of the MLV p30 protein, which is part of the MLV pseudoparticles (Figure 2B). In light of the peptide cleavage data from Figure 2A, it is unclear if this increased cleavage is mediated by furin or another cellular protease, possibly another member of the proprotein convertase (PC) family, of which furin is a member (furin is also defined as PCSK3/PC3) (Garten, 2018).

Functional analysis of virus entry using viral pseudoparticles

To assess the functional importance of the S1/S2 site for SARS-CoV-2 entry, we utilized the MLV pseudoparticles harboring specific SARS-CoV-2 spike proteins. Particles also contain a luciferase reporter that

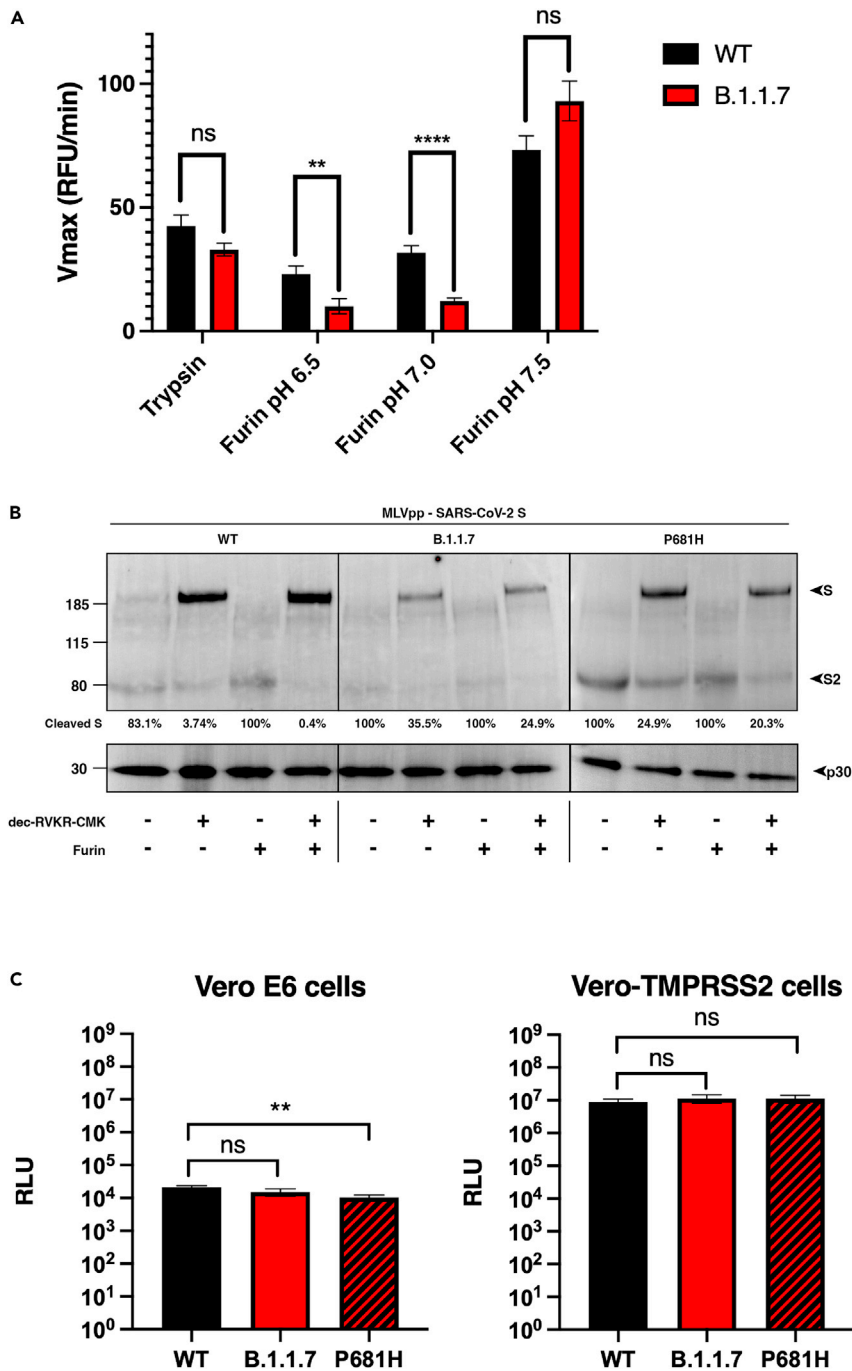


Figure 2. SARS-CoV-2 B.1.1.7 variant S1/S2 cleavage site activation and role in viral entry

(A). Fluorogenic peptide cleavage assays of the SARS-CoV-2 S1/S2 cleavage site. Peptides mimicking the S1/S2 site of the SARS-CoV-2 WT and B.1.1.7 variants were evaluated for *in vitro* cleavage by trypsin and furin proteases at pH 7.4 (trypsin) and pH 6.5, 6.0, and 7.5 (furin) conditions. A significant decrease in the cleavage of the B.1.1.7 S1/S2 peptide by furin was observed at pH 6.5 and 7.0 compared with WT. In contrast, a non-significant increase in the furin cleavage of the B.1.1.7 peptide was observed at pH 7.5. Error bars represent \pm standard errors ($n = 9$). Asterisks indicate statistical significance compared to the untreated control. Statistical analysis was performed using an unpaired Student's *t* test. ** $p < 0.01$, **** $p < 0.0001$.

(B) Western blot analysis of MLV pseudoparticles (MLVpps) carrying the WT, B.1.1.7, or P681H S. Uncleaved S (~185 kDa) and cleaved S2 (~85 kDa) detection was conducted using an antibody targeting the SARS-CoV-2 S2 domain. + dec-RVKR-

Figure 2. Continued

CMK refers to MLVpp produced in HEK-293T cells treated with 75 μ M dec-RVCR-CMK at the time of transfection. + furin refers to particles treated with 6 U of recombinant furin for 3 h at 37°C.

Ratio of the intensity of cleaved S band to uncleaved S in MLV pseudoparticles. Band intensity was normalized to the uncleaved band intensity of each pseudoparticle and cleavage ratio was calculated.

(C) Pseudoparticle infectivity assays in Vero E6 and Vero-TMPRSS2 cells. Cells were infected with MLV pseudoparticles harboring the VSV-G, SARS-CoV-2 S WT, SARS-CoV-2 S B.1.1.7 variant, SARS-CoV-2 S WT with P681H mutation. Data represent the average luciferase activity of cells of four biological replicates. No significant differences in luciferase transduction were observed between the infected cells. Error bars represent \pm standard deviation ($n = 3$). Asterisks indicate statistical significance compared to the untreated control. Statistical analysis was performed using an unpaired Student's *t* test. ** $p < 0.01$.

integrates into the host cell genome to drive expression of luciferase, which is quantifiable (Millet et al., 2019). In this study, MLV pseudoparticles containing the SARS-CoV-2 spikes of Wuhan-Hu-1 WT, B.1.1.7, and a P681H point mutant of Wuhan-Hu-1 were also generated alongside positive control particles containing the vesicular stomatitis virus (VSV) G protein, and negative control particles (Δ -Envelope) lacking envelope proteins (not shown), using the HEK293T cell line for particle production.

We examined infection of SARS-CoV-2 pseudoparticles in cell lines representative of both the "early" and "late" cell entry pathways (Figure 2C) as the entry mechanisms of SARS-CoV-2 can be highly cell-type dependent (Whittaker et al., 2021). In this study, we utilized the Vero-TMPRSS2 ("early pathway") and the Vero-E6 ("late pathway") cell lines, which are predicted to activate the SARS-CoV-2 S2' using TMPRSS2 and cathepsin L, respectively. Although Vero-TMPRSS2 cells gave overall higher luciferase signal indicative of more efficient entry, we observed little difference in infection between pseudoparticles displaying spike protein from either WT, B.1.1.7 or a P681H point mutant. As expected, VSVpp (positive control) infected both cell lines with several orders of magnitude higher luciferase units than the values reported with Δ -Envelope infection (negative control).

Viral growth in cell culture

According to our results, the P681H mutation did not provide any molecular or functional advantage for the B.1.1.7 variant entry into the host cell. However, we wanted to evaluate if the mutations in the B.1.1.7 variant will impact the viral replication of a viral isolate in cell culture (*ex vivo*). To do this, we infected Vero E6 and Vero-TMPRSS2 cells with SARS-CoV-2 strain USA-WA1/2020 or a B.1.1.7 isolate and evaluated the viral growth at 6, 12, 24, and 48 h post infection (p.i.) through TCID₅₀ and immunofluorescence (IFA) assays. We observed that the viral growth of the B.1.1.7 variant was initially slower at 12 and 24 h p.i., in Vero E6 cells, but it was equivalent to the USA-WA1/2020 growth at 48 h p.i. (Figures 3A and 3B, Vero E6 cells panels). B.1.1.7 growth in Vero-TMPRSS2 cells was similar to USA-WA1/2020 during the full course of the 48-h experiment (Figures 3A and 3B, Vero-TMPRSS2 panels). These results agree with our *in vitro* and functional assays, suggesting that the B.1.1.7 variant does not possess a replication advantage to the USA-WA1/2020 strain *ex vivo* in Vero-derived cell lines representative of both the "early" and "late" entry pathways.

Functional analysis of membrane fusion activity

It has been previously reported that the B.1.1.7 variant possesses an advantage in terms of transmission between infected and susceptible individuals (Davies et al., 2021). However, to date, our data does not show functional or replication features in the B.1.1.7 that support any change in the viral behavior and pathogenesis. Thus, we wanted to explore more directly the fusion capability of the B.1.1.7 spike protein in order to see if the P681H mutation provided any advantage for cell-to-cell transmission. To study this, we performed a cell-to-cell fusion assay where Vero-TMPRSS2 and VeroE6 cells were transfected with the WT, B.1.1.7, and Wuhan-Hu-1 P681H spike gene and we then evaluated syncytia formation as a readout of membrane fusion (Figure 4A). Although Vero-TMPRSS2 cells formed more extensive syncytia than VeroE6 cells, we observed only slight differences in the syncytia formation following spike protein expression for WT, B.1.1.7, or Wuhan-Hu-1 P681H (Figure 4B). These data show that the P681H mutation had little effect on membrane fusion activity of the SARS-CoV-2 spike protein under the conditions tested.

SARS-CoV-2 B.1.1.7 variant infection in human respiratory tract-derived cells

So far, all our results have shown no differences between B.1.1.7 and WT behavior from molecular and functional points of view. However, the functional studies were performed using susceptible cells that do not

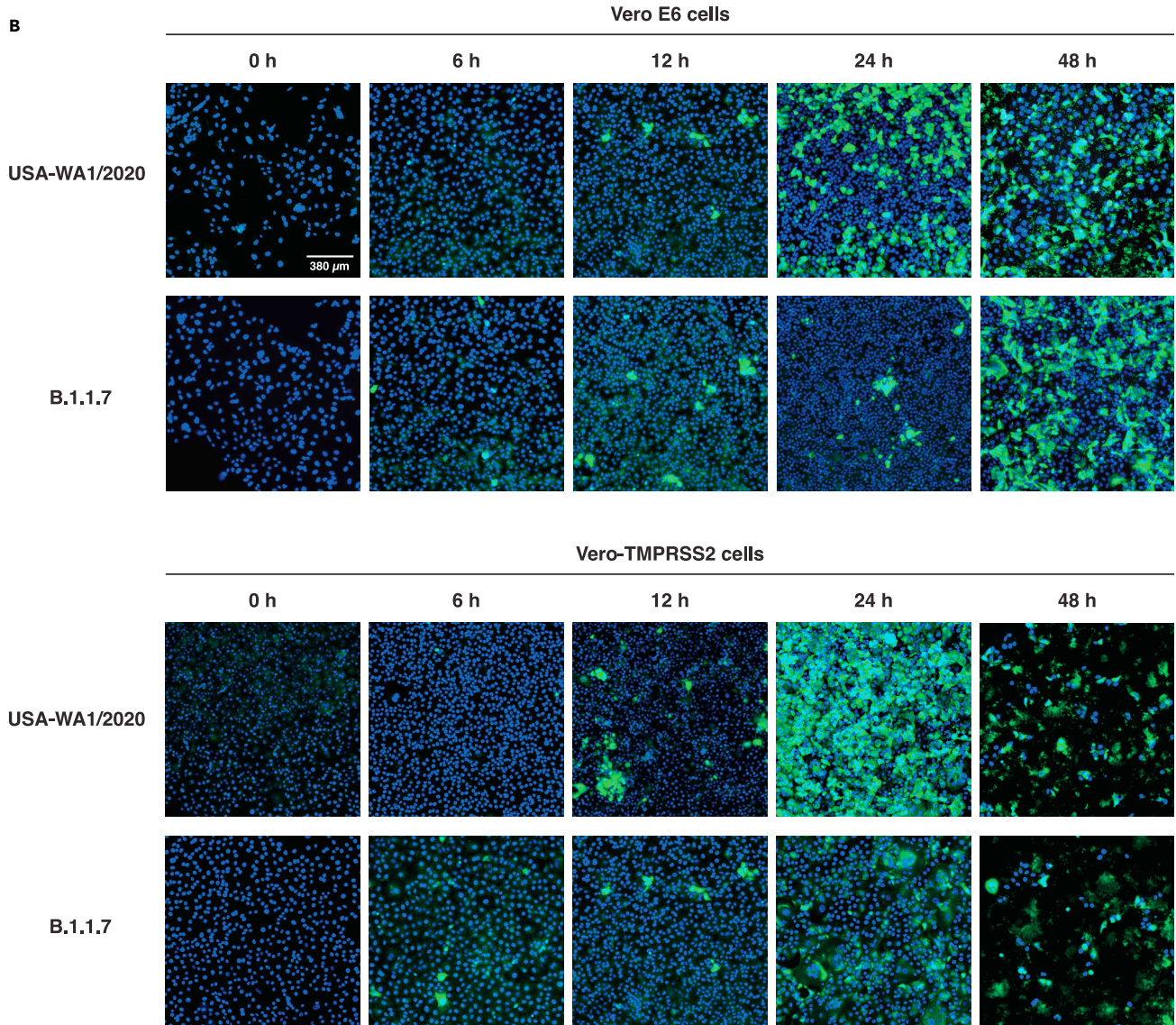
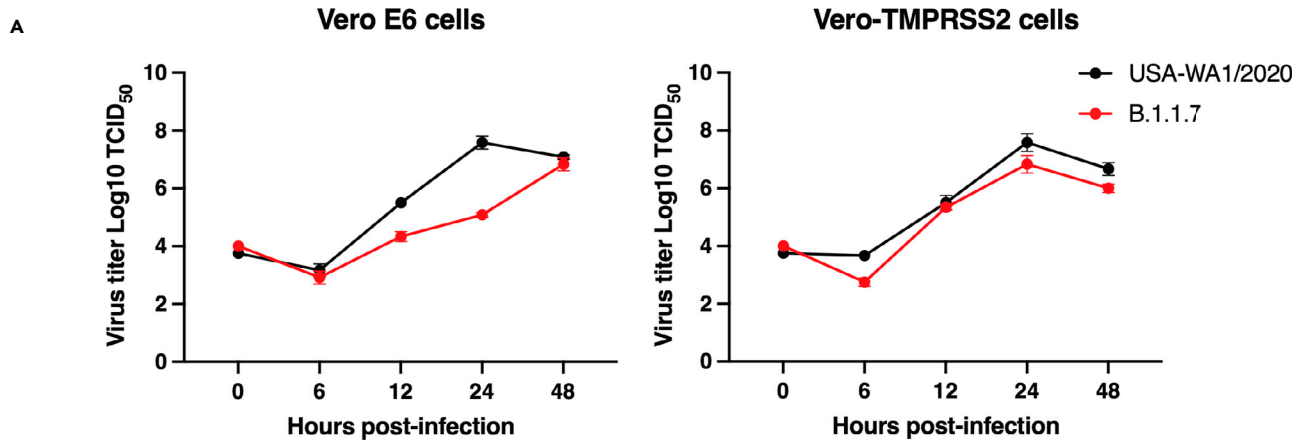


Figure 3. SARS-CoV-2 B.1.1.7 variant infectivity *ex vivo*

(A) SARS-CoV-2 WA1/2020 and B.1.1.7 growth curves on Vero E6 and Vero-TMPRSS2 cells. Cells were infected to an MOI of 0.1 and supernatant was collected at 0, 6, 12, 24, and 48 h p.i. Growth curves were then calculated using TCID₅₀. Error bars represent \pm standard deviation ($n = 3$).

(B). Immunofluorescence assay (IFA) of SARS-CoV-2 WA1/2020 and B.1.1.7 infection on Vero E6 and Vero-TMPRSS2 cells. Cells were infected to an MOI of 0.1 and IFA was performed 0, 6, 12, 24, and 48 h p.i. Detection of infected cells (green) was conducted using an antibody targeting the SARS-CoV-2 S2 domain. Cell nuclei were stained using DAPI (blue).

necessarily represent the typical cell type that the virus will initially infect *in vivo*, which are principally respiratory tract cells. To address this, we performed functional viral entry studies and live virus infection assays in respiratory-type Calu-3 cells. We used the MLV pseudoparticles harboring the WT, B.1.1.7, and mutated P681H spike proteins and infected Calu-3 cells. We observed slight but significant differences in the luciferase transduction between WT and B.1.1.7 spike-carrying pseudoparticles (Figure 5A), but no differences with the P681H mutated spike-carrying particles, compared with WT. Interestingly, we did not observe any differences in the viral growth between USA-WA1/2020 and a B.1.1.7 virus isolate in Calu-3 cells (Figure 5B), which suggests that, as with Vero E6 and Vero-TMPRSS2 cells, there is no functional advantage for B.1.1.7 in respiratory epithelial cells, i.e., Calu-3 cells.

DISCUSSION

The factors influencing increased transmissibility and pathogenicity of SARS-CoV-2 variants remain poorly understood. Here, we performed *in vitro* assays using fluorogenic peptides mimicking the S1/S2 sequence from both Wuhan-Hu-1 and the B.1.1.7 VOC and observed no definitive difference in furin cleavage for B.1.1.7. We performed functional assays using pseudo-typed particles harboring SARS-CoV-2 spike proteins and observed no significant transduction differences between Wuhan-Hu-1 and B.1.1.7 spike-carrying pseudo-typed particles in VeroE6 or Vero-TMPRSS2 cells, despite the spikes containing P681H being more efficiently cleaved. Likewise, we show no differences in cell-cell fusion assays using the spike P681H-expressing cells, as well as no notable effects on viral replication. Our findings suggest that the introduction of P681H in the B.1.1.7 variant may increase spike cleavage by furin-like proteases, but this does not significantly impact viral entry, infection, or cell-cell spread. We consider that other factors are at play to account for the increase in transmission and disease severity attributed to the SARS-CoV-2 B.1.1.7 VOC.

Overall, we show that the P681H mutation at the S1/S2 site of the SARS-CoV-2 spike protein may increase its cleavability by furin-like proteases but that this does not translate into increased virus entry or membrane fusion. These findings are broadly in line with those of Brown et al. (2021) using infectious SARS-CoV-2, who showed no differences in the B.1.1.7 variant in terms of viral replication in primary human airway cells but did show a disadvantage in Vero cells linked to increased cleavage of the spike protein. In contrast, Dicken et al. (2021) indicated enhanced entry of B.1.1.7, but in this case only under conditions with low expression of the ACE2 receptor.

B.1.1.7 is certainly not the only SARS-CoV-2 variant with a P681H change in the spike protein; it is also present in B.1.243 (clade 20A), B.1.222 (clade 20B), and a lineage B.1 variant termed clade 20C, with these three variants recently reported in New York State, USA (Lasek-Nesselquist et al., 2021). Interestingly, B.1.243 comprised the majority of P681H-containing viruses and was the predominant variant in New York in November 2020 but had declined significantly by February 2021 (to be replaced by B.1.1.7 and B.1.222 among other variants) some of which do not contain P681H (e.g., B.1.429). Other examples of variants containing P681H include A.VOI.V2 detected through travel surveillance in Angola, Africa (de Oliveira et al., 2021), isolates from Hawaii (Maison et al., 2021), and viruses originally classified under lineage B.1.1.28 in locations such as the Philippines (Tablizo et al., 2021). However, many other VOIs e.g., CAL.20C (Zhang et al., 2021a) do not contain P681H. Other variants containing mutations have been identified that have been proposed to impact S1/S2 cleavage, e.g., A688V (Tegally et al., 2021b), but we consider such mutations to be too distal to the cleavage site to have a direct impact on furin activity.

The SARS-CoV-2 S1/S2 site contains three basic residues in atypical spacing for a furin cleavage site (Tang et al., 2021) and as such is not “polybasic.” The P681H mutation increases the number of basic residues to four (especially at lowered pH) and is predicted to result in a slightly increased cleavability based on ProP and Pitou scoring and peptide cleavage assays at pH 7.4 (Figure 1A). However, it is important to note that the P681H change does not result in the formation of a consensus furin cleavage site (i.e., ^{P4}R-X-K/R-R^{P1}), even at lowered pH. It is also of note that increased spike protein cleavage does not always translate into

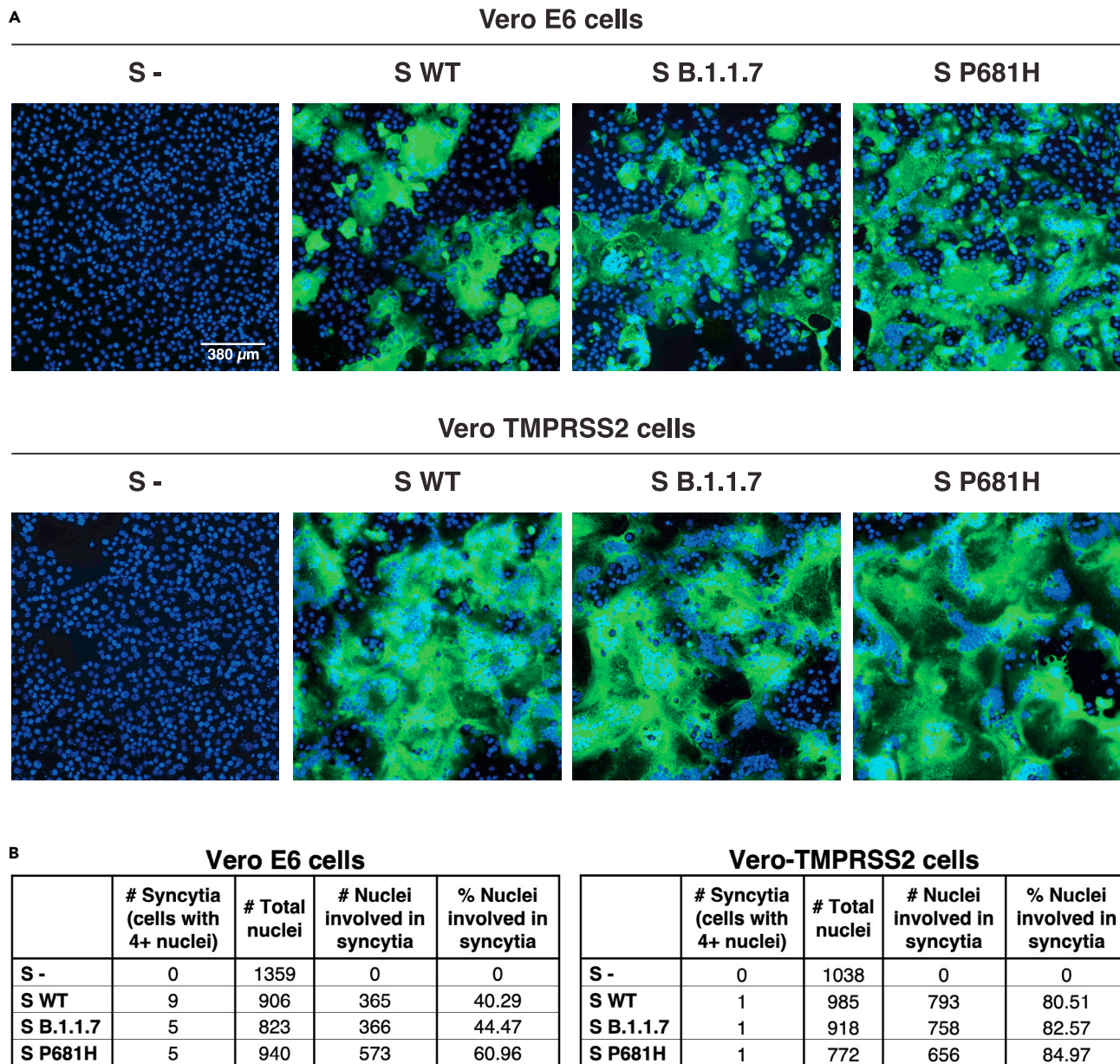


Figure 4. Cell-to-cell fusion in SARS-CoV-2 B.1.1.7 S expressing cells

(A) Cell-to-cell fusion in Vero E6 and Vero-TMPRSS2 cells expressing SARS-CoV-2 S. Cells were transfected with a plasmid carrying the WT, B.1.1.7, or P681H S gene and evaluated through IFA after 28 h. Syncytia formation was observed using an antibody targeting the SARS-CoV-2 S2 domain and a DAPI for cell nuclei (blue).

(B) Syncytia counting in SARS-CoV-2 S-expressing cells. Total number of nuclei per cell were counted to determine the percentage of nuclei involved in syncytia.

increased function and may in fact be detrimental. A good example of this is the insertion of furin cleavage sites into SARS-CoV-1 spike at S1/S2 and/or S2', which resulted in a hyper-fusogenic phenotype (Belouzard et al., 2009; Follis et al., 2006), but with pseudoparticles being unrecoverable especially when added at S2' presumably due to the presence of an unstable spike protein. One interpretation of the appearance of the P681H mutation in circulating viruses is that SARS-CoV-2 is evolving to become a transmissible but relatively benign community-acquired respiratory (CAR) or "common cold" coronavirus (Jin et al., 2020), such as the betacoronaviruses HCoV-HKU1 and HCoV-OC43, both of which have very strong "polybasic" furin cleavage sites at the S1/S2 position (Figure 1A). It remains to be determined how any increased

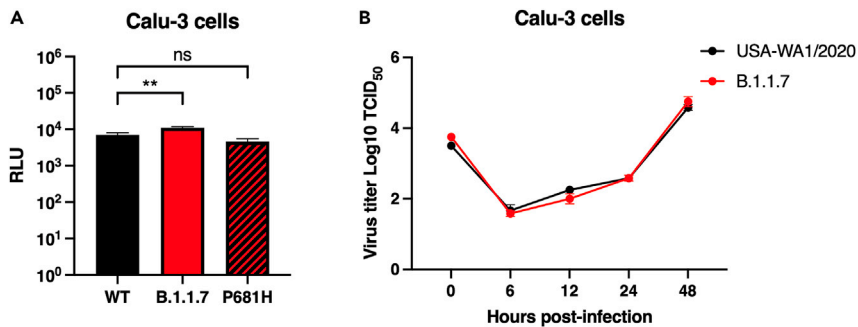


Figure 5. Infection in respiratory Calu-3 cells

(A) Pseudoparticle infectivity assays in Calu-3 cells. Cells were infected with MLV pseudoparticles harboring the VSV-G, SARS-CoV-2 S WT, SARS-CoV-2 S B.1.1.7 variant, SARS-CoV-2 S WT with P681H mutation. Data represent the average luciferase activity of cells of three biological replicates. A significant increase in the luciferase transduction was observed with the pseudoparticles harboring the B.1.1.7 S ($P = 0.0076$). Error bars represent \pm standard deviation ($n = 3$). Asterisks indicate statistical significance compared to the untreated control. Statistical analysis was performed using an unpaired Student's t test. ** $p < 0.01$.

(B) SARS-CoV-2 WA1/2020 and B.1.1.7 growth curves on Calu-3 cells. Cells were infected to an MOI of 0.1 and supernatant was collected at 0, 6, 12, 24, and 48 h p.i. Growth curves were then calculated using TCID₅₀. Error bars represent \pm standard deviation ($n = 3$).

cleavage of SARS-CoV-2 S may affect factors such as increased duration of viral shedding, which is one possible explanation of increased transmissibility for B.1.1.7 (Kissler et al., 2021).

As explained for other variants (including D614G in humans and Y453F in mink [Lauring and Hodcroft, 2021]), we consider that the rise of P681H-containing viruses could be due to chance, with founder effects being responsible for rapid progression, or P681H may confer an advantage with regards transmissibility or cell-cell spread *in vivo*. Our data here reinforce the concept that, although analysis of individual point mutations is a critical part of understanding virus biology, a full assessment of the epidemiological context of virus infection requires more extensive study (Goodman and Whittaker, 2021). It will continue to be important to track VOCs and other variants that may pose a threat for exponential spreading. Although the VOCs B.1.351 and B.1.1.28.1 (P.1) have been of high concern due to immune escape, B.1.1.7 was not considered a concern in this regard (Planas et al., 2021); however, the possible acquisition of “immune-escape” mutations such as E484K or N439K (Chan et al., 2020; Di Caro et al., 2021) remains possible. Although B.1.1.7 remains in circulation, B.1.617.2 is now outcompeting this and other variants. The three notable B.1.617 variants B.1.617.1, B.1.617.2 (Delta), and B.1.617.3, along with prior variants such as A.23.1 all contain a distinct change in the P5 position of the S1/S2 cleavage site (P681R), with early indications suggesting a growth advantage over P681H (Peacock et al., 2021; Saito et al., 2021), possibly with the replacement of the histidine in B.1.1.7 with a more conventional basic amino acid providing an important increase in viral fitness in the pathway of pandemic progression. We have recently addressed the role of the P681R mutation on the activation by furin and found that the introduction of an arginine at this position could significantly increase furin activation, potentially increasing viral entry and cell-to-cell spread (Lubinski et al., 2021). Other recent studies have also demonstrated that the P681R mutation enhances the viral replication, and the introduction of a reverse mutation to the WT genotype P681 significantly reduces the fitness of the Delta variant to levels even lower than that of the Alpha variant, which harbors the P681H mutation (Liu et al., 2021). These findings highlight the importance of the P681R mutation and provide insights in the increased fitness of B.1.617.2/Delta.

B.1.1.7 remains as a VOC as defined by the World Health Organization and has recently been moved to a “variant being monitored” as defined by the US Centers for Disease Control. Despite the current global dominance of B.1.617.2/Delta (containing P618R), other P681H-containing variants such as B.1.620 (Dudas et al., 2021) contain an even higher level of spike mutations than B.1.1.7 (11 in total, including P681H) and are expanding in certain regions of Europe and Africa, which means that the evolution of SARS-CoV-2 remains an ongoing process that needs to be carefully assessed.

Limitations of the study

Bioinformatic and *in silico* analyses are predictive and they may not be fully accurate. These tools provided the bases for the subsequent experiments, but they do not provide definite data. We used fluorogenic

Table 1. SARS-CoV-2 B.1.1.7 variant original sample and sequence submission information

Virus name	Accession number	Originating laboratory	Submitting laboratory	Authors	Submitter
hCoV-19/England/MILK-9E05B3/2020	EPI_ISL_601443	Lighthouse Lab in Milton Keynes	Wellcome Sanger Institute for the COVID-19 Genomics UK (COG-UK) consortium	The Lighthouse Lab in Milton Keynes and Alex Alderton, Roberto Amato, Sonia Goncalves, Ewan Harrison, David K. Jackson, Ian Johnston, Dominic Kwiatkowski, Cordelia Langford, John Sillitoe on behalf of the Wellcome Sanger Institute COVID-19 Surveillance Team http://www.sanger.ac.uk/covid-team	Robert Davies

peptides mimicking the SARS-CoV-2 S1/S2 regions, to evaluate the cleavage by furin and trypsin proteases. These short-length peptides do not resemble the original structural folding in the native protein, and this could result in an altered cleavage by the protease. Experiments using purified full-length protein may be needed to further evaluate the protease cleavage. The pseudoparticle system we used for the viral entry functional experiments has been broadly described and used in previous studies by our group and other researchers globally. This system provides a safe tool to study highly pathogenic viruses under biosecurity level 2 (BSL-2) conditions, as the pseudoparticles can mimic the viral entry but their replication is impaired, which eliminates the biosafety risks. Although retrovirus-based pseudoparticles are commonly used to study coronaviruses, these systems have the disadvantage that their assembly and viral envelope protein incorporation differs from the normal pathways used by coronaviruses. This may affect the amount of viral envelope protein that is incorporated to the pseudoparticles and hindering the evaluation of the viral infection. We performed live virus infection assays to corroborate our pseudoparticle data and observed a similar behavior, which suggests that the pseudoparticle system is accurate and valid, despite differential membrane envelope protein incorporation between MLV and coronaviruses.

SARS-CoV-2 can readily lose its furin cleavage site upon cell culture adaptation (Johnson et al., 2021) (Johnson et al., 2021). For our study, we did not include these controls as previous studies from our group have shown that SARS-like viruses lacking a functional S1/S2 loop rely on other proteases to facilitate entry and can have alternate entry outcomes depending on the infected cell type (Tang et al., 2021). In recent months, the emerging variant B.1.617.2 (Delta) has become the most predominant circulating SARS-CoV-2 variant and harbors a P681R mutation, which is currently the focus of ongoing studies from ourselves and other groups (Liu et al., 2021; Lubinski et al., 2021; Saito et al., 2021; Zhang et al., 2021b).

STAR★METHODS

Detailed methods are provided in the online version of this paper and include the following:

- KEY RESOURCES TABLE
- RESOURCE AVAILABILITY
 - Lead contact
 - Materials availability
 - Data and code availability
- EXPERIMENTAL MODEL AND SUBJECT DETAILS
 - Cells
- METHOD DETAILS
 - Furin prediction calculations
 - In silico homology modeling
 - Fluorogenic peptide assays
 - Synthesis and cloning of the B.1.1.7 spike protein
 - Site-directed mutagenesis
 - Pseudoparticle generation
 - Pseudoparticle infection assay
 - Western blot analysis of pseudoparticles
 - Growth curves

- Immunofluorescence assay
- Cell-cell fusion assay
- QUANTIFICATION AND STATISTICAL ANALYSIS

ACKNOWLEDGMENTS

This work was funded by the National Institutes of Health research grant R01AI35270. T.T. is supported by the National Science Foundation Graduate Research Fellowship Program under Grant No. DGE-1650441 and the Samuel C. Fleming Family Graduate Fellowship. We would especially like to thank Hector Aguiar-Carreno and Ruth Collins for important insight, and all members of the Daniel, Diel, and Whittaker groups for helpful discussions.

AUTHOR CONTRIBUTIONS

Conceptualization: B.L., T.T., S.D., J.A.J., and G.R.W.; methodology: B.L., M.H.V.F., L.F., T.T., S.D., D.G.D., J.A.J., and G.R.W.; investigation: B.L., M.H.V.F., L.F., T.T., J.A.J.; writing - original draft: B.L., T.T., J.A.J., and G.R.W.; writing - review & editing, B.L., M.H.V.F., T.T., S.D., D.G.D., J.A.J., and G.R.W.; visualization: B.L., M.H.V.F., T.T., and J.A.J.; supervision: S.D., D.G.D., J.A.J., and G.R.W.; funding acquisition: S.D. and G.R.W.

DECLARATION OF INTERESTS

The authors manifest no conflict of interest.

Received: July 14, 2021

Revised: October 15, 2021

Accepted: December 7, 2021

Published: January 21, 2022

REFERENCES

- Belouzard, S., Chu, V.C., and Whittaker, G.R. (2009). Activation of the SARS coronavirus spike protein via sequential proteolytic cleavage at two distinct sites. *Proc. Natl. Acad. Sci.* *106*, 5871–5876.
- Brown, J.C., Goldhill, D.H., Zhou, J., Peacock, T.P., Frise, R., Goonawardane, N., Baillon, L., Kugathasan, R., Pinto, A.L., McKay, P.F., et al. (2021). Increased transmission of SARS-CoV-2 lineage B.1.1.7 (VOC 202012/01) is not accounted for by a replicative advantage in primary airway cells or antibody escape. *bioRxiv*, 2021.2002.2024.432576.
- Challen, R., Brooks-Pollock, E., Read, J.M., Dyson, L., Tsaneva-Atanasova, K., and Danon, L. (2021). Risk of mortality in patients infected with SARS-CoV-2 variant of concern 202012/1: matched cohort study. *BMJ* *372*, n579.
- Chan, J.F., Yuan, S., Kok, K.H., To, K.K., Chu, H., Yang, J., Xing, F., Liu, J., Yip, C.C., Poon, R.W., et al. (2020). A familial cluster of pneumonia associated with the 2019 novel coronavirus indicating person-to-person transmission: a study of a family cluster. *Lancet* *395*, 514–523.
- Coutinho, R.M., Marquitti, F.M.D., Ferreira, L.S., Borges, M.E., da Silva, R.L.P., Canton, O., Portella, T.P., Poloni, S., Franco, C., Plucinski, M.M., et al. (2021). Model-based estimation of transmissibility and reinfection of SARS-CoV-2 P.1 variant. *Commun. Med.* *1*, 48.
- Davies, N.G., Abbott, S., Barnard, R.C., Jarvis, C.I., Kucharski, A.J., Munday, J.D., Pearson, C.A.B., Russell, T.W., Tully, D.C., Washburne, A.D., et al. (2021). Estimated transmissibility and impact of SARS-CoV-2 lineage B.1.1.7 in England. *Science* *372*, eabg3055.
- de Oliveira, T., Lutucuta, S., Nkengasong, J., Morais, J., Paixão, J.P., Neto, Z., Afonso, P., Miranda, J., David, K., Inglês, L., et al. (2021). A novel variant of interest of SARS-CoV-2 with multiple spike mutations detected through travel surveillance in Africa. *medRxiv*, 2021.2003.2030.21254323.
- Di Caro, A., Cunha, F., Petrosillo, N., Beeching, N.J., Ergonul, O., Petersen, E., and Koopmans, M.P.G. (2021). Severe acute respiratory syndrome coronavirus 2 escape mutants and protective immunity from natural infections or immunizations. *Clin. Microbiol. Infect.* *27*, 823–826.
- Dicken, S.J., Murray, M.J., Thorne, L.G., Reuschl, A.-K., Forrest, C., Ganeshalingham, M., Muir, L., Kalemera, M.D., Palor, M., McCoy, L.E., et al. (2021). Characterisation of B.1.1.7 and Pangolin coronavirus spike provides insights on the evolutionary trajectory of SARS-CoV-2. *bioRxiv*, 2021.2003.2022.436468.
- Duckert, P., Brunak, S., and Blom, N. (2004). Prediction of proprotein convertase cleavage sites. *Protein Eng. Des. Select.* *17*, 107–112.
- Dudas, G., Hong, S.L., Potter, B.I., Calvignac-Spencer, S., Niatou-Singa, F.S., Tombolomako, T.B., Fuh-Neba, T., Vickos, U., Ulrich, M., Leendertz, F.H., et al. (2021). Emergence and spread of SARS-CoV-2 lineage B.1.620 with variant of concern-like mutations and deletions. *Nat. Commun.* *12*, 5769.
- Follis, K.E., York, J., and Nunberg, J.H. (2006). Furin cleavage of the SARS coronavirus spike glycoprotein enhances cell–cell fusion but does not affect virion entry. *Virology* *350*, 358–369.
- Garten, W. (2018). Characterization of proprotein convertases and their involvement in virus propagation. In *Activation of Viruses by Host Proteases*, E. Böttcher-Friebertshäuser, W. Garten, and H. Dieter Klenk, eds. (Springer), pp. 205–248.
- Goodman, L.B., and Whittaker, G.R. (2021). Public health surveillance of infectious diseases: beyond point mutations. *Lancet Microbe.* *2*, e53–e54.
- Jaimes, J.A., Andre, N.M., Chappie, J.S., Millet, J.K., and Whittaker, G.R. (2020a). Phylogenetic analysis and structural modeling of SARS-CoV-2 spike protein reveals an evolutionary distinct and proteolytically sensitive activation loop. *J. Mol. Biol.* *432*, 3309–3325.
- Jaimes, J.A., Millet, J.K., Goldstein, M.E., Whittaker, G.R., and Straus, M.R. (2019). A fluorogenic peptide cleavage assay to screen for proteolytic activity: applications for coronavirus spike protein activation. *J. Vis. Exp.* *143*, 1–7.
- Jaimes, J.A., Millet, J.K., and Whittaker, G.R. (2020b). Proteolytic cleavage of the SARS-CoV-2 spike protein and the role of the novel S1/S2 site. *iScience* *23*, 101212.
- Jin, X., Xu, K., Jiang, P., Lian, J., Hao, S., Yao, H., Jia, H., Zhang, Y., Zheng, L., Zheng, N., et al. (2020). Virus strain from a mild COVID-19 patient in Hangzhou represents a new trend in SARS-CoV-2 evolution potentially related to Furin

- cleavage site. *Emerging microbes & infections* 9, 1474–1488.
- Johnson, B.A., Xie, X., Bailey, A.L., Kalveram, B., Lokugamage, K.G., Muruato, A., Zou, J., Zhang, X., Juelich, T., Smith, J.K., et al. (2021). Loss of furin cleavage site attenuates SARS-CoV-2 pathogenesis. *Nature* 591, 293–299.
- Kissler, S.M., Fauver, J.R., Mack, C., Tai, C.G., Breban, M.I., Watkins, A.E., Samant, R.M., Anderson, D.J., Ho, D.D., Metti, J., et al. (2021). Densely sampled viral trajectories for SARS-CoV-2 variants alpha (B.1.1.7) and epsilon (B.1.429). *medRxiv*, 2021.2002.2016.21251535.
- Lasek-Nesselquist, E., Pata, J., Schneider, E., and George, K.S. (2021). A tale of three SARS-CoV-2 variants with independently acquired P681H mutations in New York State. *medRxiv*, 2021.2003.2010.21253285.
- Lauring, A.S., and Hodcroft, E.B. (2021). Genetic variants of SARS-CoV-2—what do they mean? *JAMA* 325, 529–531.
- Liu, Y., Liu, J., Johnson, B.A., Xia, H., Ku, Z., Schindewolf, C., Widen, S.G., An, Z., Weaver, S.C., Menachery, V.D., et al. (2021). Delta spike P681R mutation enhances SARS-CoV-2 fitness over Alpha variant. *bioRxiv*, 2021.2008.2012.456173.
- Lubinski, B., Frazier, L.E., Phan, M.V.T., Bugembe, D.L., Tang, T., Daniel, S., Cotten, M., Jaimes, J.A., and Whittaker, G.R. (2021). Spike protein cleavage-activation mediated by the SARS-CoV-2 P681R mutation: a case-study from its first appearance in variant of interest (VOI) A.23.1 identified in Uganda. *bioRxiv*, 2021.2006.2030.450632.
- Maison, D.P., Ching, L.L., Shikuma, C.M., and Nerurkar, V.R. (2021). Genetic characteristics and phylogeny of 969-bp S gene sequence of SARS-CoV-2 from Hawaii reveals the worldwide emerging P681H mutation. *bioRxiv*, 2021.2001.2006.425497.
- Millet, J.K., Tang, T., Nathan, L., Jaimes, J.A., Hsu, H.L., Daniel, S., and Whittaker, G.R. (2019). Production of pseudotyped particles to study highly pathogenic coronaviruses in a biosafety level 2 setting. *J. Vis. Exp.* 145, 1–9.
- Nelson, D.L., and Cox, M.M. (2000). *Lehninger Principles of Biochemistry* (Worth Publishers).
- Peacock, T.P., Goldhill, D.H., Zhou, J., Baillon, L., Frise, R., Swann, O.C., Kugathasan, R., Penn, R., Brown, J.C., Sanchez-David, R.Y., et al. (2020). The furin cleavage site of SARS-CoV-2 spike protein is a key determinant for transmission due to enhanced replication in airway cells. *bioRxiv*, 2020.2009.2030.318311.
- Peacock, T.P., Sheppard, C.M., Brown, J.C., Goonawardane, N., Zhou, J., Whiteley, M., de Silva, T.I., and Barclay, W.S. (2021). The SARS-CoV-2 variants associated with infections in India, B.1.617, show enhanced spike cleavage by furin. *bioRxiv*, 2021.2005.2028.446163.
- Planas, D., Bruel, T., Grzelak, L., Guivel-Benhassine, F., Staropoli, I., Porrot, F., Planchais, C., Buchrieser, J., Rajah, M.M., Bishop, E., et al. (2021). Sensitivity of infectious SARS-CoV-2 B.1.1.7 and B.1.351 variants to neutralizing antibodies. *Nat. Med.* 27, 917–924.
- Polgár, L. (1989). General aspects of proteases. In *Mechanisms of Protease Action* (CRC press), pp. 43–86.
- Rambaut, A., Loman, N., Pybus, O., Barclay, W., Barrett, J., Carabelli, A., Connor, T., Peacock, T., Robertson, D.L., and Volz, E. <https://virological.org/t/preliminary-genomic-characterisation-of-an-emergent-sars-cov-2-lineage-in-the-uk-defined-by-a-novel-set-of-spike-mutations/563>.
- Saito, A., Irie, T., Suzuki, R., Maemura, T., Nasser, H., Uriu, K., Kosugi, Y., Shirakawa, K., Sadamasu, K., Kimura, I., et al. (2021). SARS-CoV-2 spike P681R mutation, a hallmark of the Delta variant, enhances viral fusogenicity and pathogenicity. *bioRxiv*, 2021.2006.2017.448820.
- Seidah, N.G., and Prat, A. (2012). The biology and therapeutic targeting of the proprotein convertases. *Nat. Rev. Drug Discov.* 11, 367–383.
- Tablizo, F.A., Kim, K.M., Lapid, C.M., Castro, M.J.R., Yangzon, M.S.L., Maralit, B.A., Ayes, M.E.C., Cutiongco-de la Paz, E.M., De Guzman, A.R., Yap, J.M.C., et al. (2021). Genome sequencing and analysis of an emergent SARS-CoV-2 variant characterized by multiple spike protein mutations detected from the Central Visayas Region of the Philippines. *medRxiv*, 2021.2003.2003.21252812.
- Tang, T., Jaimes, J.A., Bidon, M.K., Straus, M.R., Daniel, S., and Whittaker, G.R. (2021). Proteolytic activation of SARS-CoV-2 spike at the S1/S2 boundary: potential role of proteases beyond furin. *ACS Infect. Dis.* 7, 264–272.
- Tegally, H., Wilkinson, E., Giovanetti, M., Iranzadeh, A., Fonseca, V., Giandhari, J., Doolabh, D., Pillay, S., San, E.J., Msomi, N., et al. (2021a). Detection of a SARS-CoV-2 variant of concern in South Africa. *Nature* 592, 438–443.
- Tegally, H., Wilkinson, E., Lessells, R.J., Giandhari, J., Pillay, S., Msomi, N., Mlisana, K., Bhiman, J.N., von Gottberg, A., Walaza, S., et al. (2021b). Sixteen novel lineages of SARS-CoV-2 in South Africa. *Nat. Med.* 27, 440–446.
- Tian, S., Huajun, W., and Wu, J. (2012). Computational prediction of furin cleavage sites by a hybrid method and understanding mechanism underlying diseases. *Sci. Rep.* 2, 261.
- Volz, E., Mishra, S., Chand, M., Barrett, J.C., Johnson, R., Geidelberg, L., Hinsley, W.R., Laydon, D.J., Dabrera, G., O’Toole, A., et al. (2021). Assessing transmissibility of SARS-CoV-2 lineage B.1.1.7 in England. *Nature* 593, 266–269.
- Whittaker, G.R., Daniel, S., and Millet, J.K. (2021). Coronavirus entry: how we arrived at SARS-CoV-2. *Curr. Opin. Virol.* 47, 113–120.
- Zhang, W., Davis, B.D., Chen, S.S., Sincuir Martinez, J.M., Plummer, J.T., and Vail, E. (2021a). Emergence of a novel SARS-CoV-2 variant in Southern California. *JAMA* 325, 1324–1326.
- Zhang, J., Xiao, T., Cai, Y., Lavine, C.L., Peng, H., Zhu, H., Anand, K., Tong, P., Gautam, A., Mayer, M.L., et al. (2021b). Membrane fusion and immune evasion by the spike protein of SARS-CoV-2 Delta variant. *bioRxiv*, eabl9463.
- Zhou, B., Thao, T.T.N., Hoffmann, D., Taddeo, A., Ebert, N., Labroussaa, F., Pohlmann, A., King, J., Steiner, S., Kelly, J.N., et al. (2021). SARS-CoV-2 spike D614G change enhances replication and transmission. *Nature* 592, 122–127.

STAR★METHODS

KEY RESOURCES TABLE

REAGENT or RESOURCE	SOURCE	IDENTIFIER
Antibodies		
SARS-CoV-1 (2019-nCoV) Spike S2, Rabbit PAb	Sino Biological Inc.	Cat# 40590-T62
Ms mAb to MLV p30 [4b2]	Abcam	Cat# ab 130757
Bacterial and virus strains		
XL 10-Gold ultracompetent cells	Agilent	cat#200315
SARS-CoV-2 WA1/2020	Isolated by the Diel lab at the Cornell Animal Health Diagnostic Laboratory	N/a
SARS-CoV-2 B.1.1.7	Isolated by the Diel lab at the Cornell Animal Health Diagnostic Laboratory	N/a
Chemicals, peptides, and recombinant proteins		
SARS-CoV-2 WT S1/S2 Fluorogenic Peptide	Biomatik	Custom peptide synthesis - Amino Acid Sequence: TNSPRRARSVA, gross weight: 5 mg, HPLC purity: 95%, Modifications: MCA/Lys(DNP) FRET pair
SARS-CoV-2 B.1.1.7 S1/S2 Fluorogenic Peptide	Biomatik	Custom peptide synthesis - Amino Acid Sequence: TNSHRRARSVA, gross weight: 5 mg, HPLC purity: 95%, Modifications: MCA/Lys(DNP) FRET pair
Critical commercial assays		
QuikChange Lightning Site-Directed Mutagenesis Kit	Agilent Technologies, Inc.	Cat# 210518
HiSpeed Plasmid Midi Kit	Qiagen N.V.	Cat# 12643
Luciferase Assay System	Promega Co.	Cat# E1500
Experimental models: Cell lines		
Vero E6 cells	ATCC	Cat# CRL-1586
Vero TMPRSS2 cells	JCRB Cell Bank	Cat# JCRB1819
Calu3 cells	ATCC	Cat# HTB-55
Hek293T cells	ATCC	Cat# CRL-3216
Oligonucleotides		
P681H Forward Mutation Primer	Integrated DNA Technologies	cagacctggctctctgtgggagttgtctgggt
P681H Reverse Mutation Primer	Integrated DNA Technologies	accagacaaactccccacaggagccagggtctg
Sequencing primer for P681H mutation	Integrated DNA Technologies	gacgtgaattgtaccggaggtgcc
Software and algorithms		
ProP 1.0	https://services.healthtech.dtu.dk/service.php?ProP-1.0	N/a
PiTou V3	http://www.nuolan.net/reference.html	N/a
Other		
pCAGGS-VSV-G Plasmid	Michael Whitt, University of Tennessee USA	
pcDNA 3.1+	Invitrogen	Cat# V79020
pcDNA3-EGFP	Addgene	Cat# 13031
pcDNA-SARS-2 WT S	David Veesler, University of Washington USA	N/a

(Continued on next page)

Continued

REAGENT or RESOURCE	SOURCE	IDENTIFIER
pcDNA-SARS-2 WT S P681H	Gary Whittaker, Cornell University	N/a
pcDNA 3.1+ SARS-2 B.1.1.7 S	GenScript Biotech Co.	B.1.1.7 spike gene from isolate hCoV-19/England/MILK-9E05B3/2020 (EPI_ISL_601443) was codon-optimized, synthesized and cloned into a pcDNA 3.1+ vector
pTG-Luc	Jean Dubuisson, Institut Pasteur de Lille	N/a
pCMV-MLV gag-pol	Jean Dubuisson, Institut Pasteur de Lille	N/a

RESOURCE AVAILABILITY

Lead contact

If you have a request for more information or resources related to this paper, please reach out to Gary Whittaker (grw7@cornell.edu).

Materials availability

Plasmids that were generated during this study are available from the Whittaker Lab by request.

Data and code availability

All data reported in this paper will be shared by the lead contact upon request.

This paper does not report original code.

Any additional information required to reanalyze the data reported in this paper is available from the lead contacts upon request.

EXPERIMENTAL MODEL AND SUBJECT DETAILS

Cells

All cell lines were grown at 37°C with 5% CO₂. Vero E6 (ATCC CRL-1586) and Hek293T (ATCC CRL-3216) cells were grown in Dulbecco's Modified Eagle's Medium (DMEM)(Corning) with 10% HyClone™ FetalClone® II (Cytiva), and 1% HEPES (Corning). Vero TMPRSS2 cells (JCRB Cell Bank JCRB1819) were grown in DMEM, 10% Hyclone, 1% HEPES, and 1% Geneticin (Gibco). Calu3 (ATCC HTB-55) cells were grown in Eagle's Minimum Essential Medium (EMEM) (Corning) with 10% Fetal Bovine Serum (FBS)(Gibco).

METHOD DETAILS

Furin prediction calculations

Prop: CoV sequences were analyzed using the ProP 1.0 Server hosted at: <https://services.healthtech.dtu.dk/service.php?ProP-1.0>. PiTou: CoV sequences were analyzed using the PiTou V3 software hosted at: <http://www.nuolan.net/reference.html>.

In silico homology modeling

SARS-CoV-2 S protein models for Wuhan Hu-1 (GenBank accession # MN908947.3) and B.1.1.7 hCoV-19/England/MILK-9E05B3/2020 (GISAID accession # EPI_ISL_601443 – Original sample and sequence submission information included in [Table 1](#)), were built using UCSF Chimera (v.1.14, University of California) through the homology modeling tool of the Modeller extension (v.10.1, University of California) as described in ([Jaimes et al., 2020a](#)). Models were built based on the SARS-CoV S structure (PDB No. 5X58).

Fluorogenic peptide assays

Fluorogenic peptide assays were performed as described previously with minor modifications ([Jaimes et al., 2019](#)). Each reaction was performed in a 100 µL volume consisting of buffer, protease, and SARS-CoV-2 S1/S2 WT (TNSPRRARSVA) or SARS-CoV-2 S1/S2 B.1.1.7 (TNSHRRARSVA) fluorogenic peptide in an opaque 96-well plate. For trypsin catalyzed reactions, 0.8 nM/well TPCK trypsin was diluted in PBS

buffer. For furin catalyzed reactions, 1 U/well recombinant furin was diluted in buffer consisting of 20 mM HEPES, 0.2 mM CaCl₂, and 0.2 mM β-mercaptoethanol, at pH 6.5, 7.0 or 7.5. Fluorescence emission was measured once per minute for 60 minutes using a SpectraMax fluorometer (Molecular Devices, Inc.) at 30 °C with an excitation wavelength of 330 nm and an emission wavelength of 390 nm. V_{max} was calculated by fitting the linear rise in fluorescence to the equation of a line.

Synthesis and cloning of the B.1.1.7 spike protein

The B.1.1.7 spike gene from isolate hCoV-19/England/MILK-9E05B3/2020 (EPI_ISL_601443) was codon-optimized, synthesized and cloned into a pcDNA 3.1+ vector for expression (GenScript Biotech Co.).

Site-directed mutagenesis

Mutagenesis primers (cagacctggctctctgtggagttgtctggg/ acccagacaaactccacaggagagccaggtctg) were designed based on the DNA sequence for SARS-CoV-2 Wuhan-Hu-1 using the QuickChange Primer Design tool (Agilent Technologies, Inc.). Mutagenesis was carried out on a pCDNA-SARs2 Wuhan-Hu 1 S plasmid to create the P681H mutation, using the QuickChange Lightning Mutagenesis kit (Agilent Technologies, Inc.). The original plasmid was generously provided by David Veessler, University of Washington USA. XL-10 gold competent cells were transformed with the mutated plasmid, plated on LB Agar + Ampicillin plates, and left at 37°C overnight. A distinct colony was chosen the next day to grow up a 4 ml small culture at 37°C overnight. pCDNA-SARS-CoV-2 Wuhan-Hu-1 P681H S plasmid was then extracted using the QIAprep Spin Miniprep Kit (Qiagen N.V.) and Sanger sequencing was used to confirm incorporation of the mutation.

Pseudoparticle generation

HEK-293T cells were seeded at 3x10⁵ cells/ml in a 6-well plate the day before transfection. Transfection was performed using polyethylenimine (PEI) and 1X Gibco® Opti-Mem (Life Technologies Co.). Cells were transfected with 800ng of pCMV-MLV *gag-pol*, 600ng of pTG-Luc, and 600 ng of a plasmid containing the viral envelope protein of choice. Viral envelope plasmids included pCAGGS-VSV G as a positive control, pCDNA-SARS-CoV-2 Wuhan-Hu-1 S, pCDNA- SARS-CoV-2 (Wuhan-Hu-1) P681H S, and pCDNA-SARS-CoV-2 B.1.1.7 S. pCAGGS empty vector was used for a Δ-Envelope negative control. 48 hours post transfection, the supernatant containing the pseudoparticles was removed, centrifuged to remove cell debris, filtered, and stored at -80°C. For + dec-RVKR-CMK particles, 7.5 μL of dec-RVKR-CMK was added to cells immediately after transfection. pCAGGS-VSV G was generously provided by Michael Whitt, University of Tennessee USA.

Pseudoparticle infection assay

Vero E6 and Vero-TMPRSS2 cells were seeded at 3x10⁵ cells/ml in a 24 well plate the day before infection. Cells were washed three times with 1X DPBS and then infected with 200 μl of either VSV G, SARS-CoV-2 S, SARS-Cov-2 P681H S, SARS-CoV-2 B.1.1.7 S, or Δ-Envelope pseudoparticles. Infected cells incubated on a rocker for 1.5 hours at 37°C, then 300 μl of complete media were added and cells were left at 37°C. At 72 hours post-infection, cells were lysed and the level of infection was assessed using the Luciferase Assay System (Cat: E1501, Promega Co.). The manufacturer's protocol was modified by putting the cells through 3 freeze/thaw cycles after the addition of 100 μl of the lysis reagent. 10 μl of the cell lysate were added to 20 μl of luciferin, and then luciferase activity was measured using the Glomax 20/20 luminometer (Promega Co.). Infection assays were done in triplicate and were replicated 4 times. All four replicates were carried out using pseudoparticles generated from the same transfection.

Western blot analysis of pseudoparticles

3 mL of pseudoparticles were pelleted using a TLA-55 rotor with an Optima-MAX-E ultracentrifuge (Beckman Coulter, Inc.) for 2 hours at 42,000 rpm at 4°C. Untreated particles were resuspended in 30 μL DPBS buffer. For the + furin treated MLVpps, particles were resuspended in 30 μL of furin buffer consistent in 20 mM HEPES, 0.2 mM CaCl₂, and 0.2 mM β-mercaptoethanol (at pH 7.0). Particles were later incubated with 6 U of recombinant furin for 3 hours at 37°C. Sodium dodecyl sulfate (SDS) loading buffer and DTT were added to samples and samples were stored at -20°C. Immediately before running them out on the gel, samples were boiled at 95°C for 10 minutes. Samples were separated on NuPAGE Bis-Tris gel (Cat: NP0321BOX, Invitrogen Co.) and transferred on polyvinylidene difluoride (PVDF) membranes (MilliporeSigma). SARS-CoV-2 S was detected using a rabbit polyclonal antibody against the S2 domain

(Cat: 40590-T62, Sino Biological, Inc) and an AlexaFluor™ 488 goat anti-rabbit antibody (Invitrogen Co, USA). Bands were detected using the ChemiDoc (Bio-Rad Laboratories, Inc.) and band intensity was calculated using the analysis tools on Image Lab 6.1 software (Bio-Rad Laboratories, Inc.) to determine the un-cleaved-to-cleaved S ratios.

Growth curves

SARS-CoV-2 WA1/2020 and B.1.1.7 growth curves were performed in Vero E6, Vero-TMPRSS2 and Calu-3 cells. Cells were cultured in 24-well plates in advance, inoculated with a multiplicity of infection (MOI) of 0.1 and harvested at 6-, 12-, 24- and 48-hours post-infection (p.i.) in triplicate. Virus titers were determined on each time by limiting dilutions in Vero E6 cells. At 48-hours p.i. cells were fixed (3.7% formaldehyde), permeabilized (0.2% Triton-X), and stained with an anti-NP SARS-CoV-2 rabbit polyclonal antibody (produced and characterized in Diel laboratory) and then incubated with a goat anti-rabbit IgG secondary antibody (Alexa Fluor 594; Immunoreagents). Viral titers were determined by the Spearman and Karber's method and expressed as tissue culture infectious dose 50 (TCID₅₀) per milliliter.

Immunofluorescence assay

Vero E6 and Vero-TMPRSS2 cells cultured in 4-well glass slides were infected with SARS-CoV-2 WA1/2020 and B.1.1.7 (MOI = 0.1). At 0-, 6-, 12-, 24- and 48-hours p.i. cells were fixed using 3.7% formaldehyde in PBS (pH 7.2) for 30 min. The cells were washed three times with PBS and quenched with 50 mM NH₄Cl. Permeabilization was performed with 0.1% Triton X-100 in PBS for 5 minutes on ice. Blocking was performed using 5% heat inactivated goat serum in PBS for 20 minutes and the antibodies for labeling were diluted in the same solution. The spike expression was detected using the SARS-CoV-2 spike antibody (Cat: 40591-T62, Sino Biological Inc.) at 1/500 dilution for 1 hour. Secondary antibody labeling was performed using AlexaFluor™ 488 goat anti-rabbit IgG antibody (Cat: A32731, Invitrogen Co.) at a 1/500 dilution for 45 minutes. Three washes with PBS were performed between each step of the assay. Finally, slides were mounted using DAPI Fluoromount-G® (Cat: 0100-20, SouthernBiotech Inc.) and analyzed with fluorescence.

Cell-cell fusion assay

Vero E6 and Vero-TMPRSS2 cells were transfected with a plasmid harboring the spike gene of the SARS-CoV-2 Wuhan-Hu 1, SARS-CoV-2 B.1.1.7, the SARS-CoV-2 P681H S, or a delta-spike pCDNA3.1+ plasmid and evaluated through an immunofluorescence assay (IFA). Transfection was performed on 8-well glass slides at 90% confluent cells using Lipofectamine® 3000 (Cat: L3000075, Invitrogen Co.), following the manufacturer's instructions and a total of 250 ng of DNA per well was transfected. The cells were then incubated at 37°C with 5% of CO₂ for 28 hours. Syncytia was visualized through an immunofluorescence assay using the method described in the previous section. Representative images of each treatment group were taken, and these images were used to calculate the percent of nuclei involved in the formation of syncytia. Images were taken at 20X on the Echo Revolve fluorescent microscope (Model: RVL-100-M). The nuclei were counted manually using the Cell Counter plugin in ImageJ (<https://imagej.nih.gov/ij/>). Cells that expressed the spike protein and contained 4 or more nuclei were considered to be one syncytia.

QUANTIFICATION AND STATISTICAL ANALYSIS

All statistical analysis was performed using GraphPad Prism for Mac OS X, GraphPad Software, San Diego, California USA, www.graphpad.com. Two sample T-tests were used to compare SARS-CoV-2 Wuhan-Hu 1 to SARS-CoV-2 B.1.1.7 or SARS-CoV-2 P681H, with significant P values reported in the figure legends. Standard deviation was calculated and included in graphs when appropriate.